

Cite this: *J. Mater. Chem. A*, 2020, **8**, 196

Enhancing the selectivity of Nafion membrane by incorporating a novel functional skeleton molecule to improve the performance of direct methanol fuel cells†

Jialin Li,^a Fanzhe Bu,^b Chunyu Ru,^a Hao Jiang,^a Yuting Duan,^a Yinan Sun,^a Xingtong Pu,^a Lichao Shang,^a Xifang Li^a and Chengji Zhao^{*ac}

Conventional fillers have limitations on the modification of proton exchange membranes because of differences in the sizes and physicochemical properties of matrix molecules. Designing skeleton molecules is a vital way to address the limitations by enabling precise distribution in the matrix and inducing automatic nanoscale aggregation and separation of hydrophilic–hydrophobic phases. In this work, a novel SDF-PAEK polymer was synthesized with a rigid hydrophobic backbone, short high-density trifluoromethyl side chains and long flexible aliphatic pendant side chains as a skeleton molecule for the Nafion membrane. Due to the unique molecular interaction selectivity during the membrane formation process, SDF-PAEK automatically matches the Nafion molecular conformation by self-assembly. Combining an improved solution formulation and membrane-casting method, the degree of composition can therefore rise to 20%, which can effectively reduce the cost. Morphological studies show that there is a certain degree of bicontinuous phase microcrystalline domains, and the proton transport channels are highly concentrated. In contrast to the Nafion membrane, SDF-PAEK@Nafion-15% exhibits better performances with higher selectivity ($9.73 \times 10^4 \text{ S s cm}^{-3}$) and single-cell maximum power density ($\text{PD}_{\text{max}}=139 \text{ mW cm}^{-2}$, at $80 \text{ }^\circ\text{C}$), which demonstrates the feasibility of SDF-PAEK as a novel PEM skeleton molecule for fuel cell applications.

Received 16th September 2019
Accepted 25th November 2019

DOI: 10.1039/c9ta10215a

rsc.li/materials-a

Introduction

Over the past several decades, scientists have realised that an effective way to improve the single-cell performance of direct methanol fuel cells (DMFCs) is to improve the proton conductivity of its key component, the proton exchange membrane (PEM). Therefore, various membrane materials with hydrophilic groups were investigated, including fabricated macromolecules containing hydrophilic side chains,^{1–3} cross-linked membranes,^{4–6} and porous organic protogenic polymers.^{7–9} However, it is challenging to form flat interconnected hydrophilic nanoscale conduction channels even in the porous

membranes created with only one type of molecule. In those membranes, mass transport relies on discontinuous ion clusters separated from each other in hydrophobic domains, which obviously hinders proton conductivity.^{10,11} Therefore, an improvement strategy is to introduce a variety of water-retaining particles, such as inorganic oxide particles,^{12–14} heteropoly acid,^{15–17} and graphene oxides,^{18,19} to enhance the hydrophilic nature of the membranes. In this way, the number of hydration molecules in hydrophilic channels increases, which increases the proton conductivity of membranes significantly. However, due to the differences in sizes, gravity, and physicochemical properties between the particles and membrane matrix, the fillers tend to agglomerate during the membrane-casting process (even in the solvent-drying process). The subsequent discrete ion cluster phases growing around the particles also generate a degree of separation away from the membrane. This can seriously affect the performance of DMFCs.^{20–22}

Incorporating macromolecule fillers with a particular conductive ability into matrix molecules can reduce the filler loss problem and form hydrophilic phases because of physical crosslinking, and stable chemical and ionic bonds between the filler and matrix molecules.^{3,23,24} However, because the differences in molecular morphologies generate thermodynamic

^aAlan G. MacDiarmid Institute, College of Chemistry, Jilin University, Changchun 130012, People's Republic of China. E-mail: jialinmury@163.com

^bChangchun Institute of Applied Chemistry, Chinese Academy of Sciences, Changchun 130022, People's Republic of China

^cKey Laboratory of Advanced Batteries Physics and Technology (Ministry of Education), Jilin University, Changchun 130012, PR China

† Electronic supplementary information (ESI) available: ¹H NMR spectrum of DMNF; TGA curves of membranes; cross-sectional SEM images of different membranes; photographs of composite membranes; Nyquist plots of single cell impedance spectra; liquid uptake and swelling ratio of membranes; the polarization and power density curves of membranes at 25 °C. See DOI: 10.1039/c9ta10215a

immiscibility, the degree of mixing is usually low (<10 wt%), which leads to separation among the hydrophilic ion clusters on the dissimilar structures and makes them stay too far to form connected hydrophilic proton transport channels. Moreover, the performance improvements mostly depend on the chemical regulation of chain structures whereas the physical blending of polymers and ion nanoscale channels are rarely chemically modified.^{3,7,25–27} The skeleton molecule is one kind of organic composite component which is different from conventional fillers. Synthesized by matching the matrix molecule structure and resembling a skeleton of the matrix, these skeleton molecules enhance the mechanical properties of composite membranes and show a distinctive predominance for functional groups with specific characteristics. The matched molecular structures, sizes, and flexibilities can improve the thermodynamic compatibility and selectivity of the molecular interactions between the skeleton molecules and the matrix molecules in the membrane-casting process. Additionally, while enhancing some of the specific properties of the membrane materials, the adjustable chemical affinity also allows the skeleton molecule to simultaneously contribute a somewhat better material performance.

At present, Nafion, a state-of-the-art perfluorosulfonic acid molecule with a flexible aliphatic carbon main chain structure, exhibits a high proton conductivity ($\approx 0.1 \text{ S cm}^{-1}$) but also high solvent dependence and low molecular rigidity.^{1,28} A small quantity of water loss can cause the nanoscale proton transport channels to shrink and collapse quickly.^{29–31} Herein, this paper reports a novel type of proton-conducting polymer to be used as the skeleton molecule containing a hydrophobic domain—a rigid phenyl and naphthyl ring backbone and high-density of short, rigid trifluoromethyl side chains; and a hydrophilic domain—long flexible hydrophilic aliphatic side chains that are similar to Nafion. After incorporating the skeleton into the Nafion matrix at the molecular level, the methanol permeability of the membranes can be reduced by over 50%. In contrast to the conventional mixed filler-matrix, the degree of compatibility between the two molecules is also greatly improved by adjusting the solution formulation and optimizing the membrane-casting method. Inside the membranes, skeleton molecules guide the Nafion molecule to automatically form hydrophilic–hydrophobic ionic nanophase separation. Hydrophilic ion clusters aggregate to create proton transport channels with a certain connectivity. This unique nanophase separation–aggregation structure is formed by the entropy-driven self-assembly of amphiphathic sulfonated poly(arylene ether ketone) (SPAEK) chains prearranged in the casting process.

Experimental section

Materials

2,6-Dimethoxynaphthalene, 4-fluorobenzoyl chloride, 3,5-di(trifluoromethyl) aniline, and 1,4-benzoquinone were purchased from Sigma-Aldrich. Boron tribromide (BBr_3), 1,4-butanediol and sodium hydride (NaH) (60%) were purchased from Aladdin Scientific Co. Ltd, Shanghai. Zinc powder (Shanghai Chemical Reagent Co. Ltd, 95%);

hydrochloric acid (Sinopharm Chemical Reagent Co. Ltd, 37%), 1,2-dichloroethane (Shanghai Chemical Reagent Co. Ltd). *N,N*-Dimethylacetamide (DMAc), dimethylsulfoxide (DMSO), and *N*-methyl-2-pyrrolidone (NMP), used as solvents, were vacuum-distilled before use. Nafion powder was obtained by evaporating the commercial solvent D2020 (20 wt%).

Synthesis of the monomer

In a 200 mL beaker, 3,5-di(trifluoromethyl) aniline (5.7 g) and concentrated hydrochloric acid (10 mL) were stirred until they were dissolved in 100 mL water at 10 °C. And then sodium nitrite solution (1.8 g sodium nitrite in 10 mL water) was added dropwise into the aniline solution. After stirring for 1 hour, the solution underwent filtration and the filtrate was then slowly added from a dropping funnel to a 1000 mL beaker containing 1,4-benzoquinone (1.6 g) and sodium bicarbonate (10.5 g) at 5–10 °C. After a 4 hour stirring process, the product was thoroughly washed with deionized water and allowed to dry out naturally. Afterward, the product (7.1 g), zinc powder (4.3 g), deionized water (43 mL) and toluene (64 mL) were added into a four-necked flask equipped with a mechanical stirrer, a thermometer, a nitrogen inlet and a Dean–Stark apparatus with a reflux condenser. After refluxing for 6 hours at 80 °C, the hot mixture was then filtered. And the crude was dried and recrystallized from methanol to give grey needles of DFBP.

Synthesis of DF-PAEK

1,5-Bis(4-fluorobenzoyl)-2,6-dimethoxynaphthalene (DMNF) (12.97 g, 30 mmol), DFBP (7.56 g, 30 mmol), K_2CO_3 (4.56 g, 33 mmol), tetramethylene sulfone (50 mL) and toluene (10 mL) were dissolved in a three-necked flask with continuous stirring in a nitrogen atmosphere. The solution was then heated to 120 °C for 2 hours until the water by-product generated in the polymerization step was eliminated. While the toluene was slowly drained, the temperature was gradually raised to 200 °C, and the reaction was sustained for 12 hours. Then, the viscous product was washed with deionized water. The product was finally dried at 60 °C for 48 hours and ultimately named DF-PAEK.

Synthesis of SDF-PAEK

The grafting of flexible pendent sulfonated groups onto the polymer was performed according to a procedure reported previously.^{32,33} DF-PAEK (5 g, 7.1 mmol) was dissolved in 125 mL refined dichloromethane, and then 1 M BBr_3 -dichloromethane solution (20 mL) was dropwise added into that flask. After the reaction sustained for 24 hours, 500 mL aqueous ethanol solution was added into the system for quenching. The collected brick red product, named OH-DF-PAEK, was washed with deionized water. Then pure OH-DF-PAEK (2.49 g, 3.56 mmol), NaH (0.568 g, 14.26 mmol) and 1,4-butanediol (3.1 mL, 30 mmol) were dissolved in 50 mL DMSO in a nitrogen atmosphere with constant stirring at 85 °C for 8 hours. Finally, the solution was poured into acetone to precipitate the product. The solid SDF-PAEK was obtained after acetone purification.

Preparation of SDF-PAEK@Nafion-x composite membranes

This paper employs a solution method different from the usual method to cast membranes. As shown in Scheme 1, dry Nafion powder was dissolved in DMSO as the casting solution with a concentration of 10 wt%. After being stirred for 72 hours, the DF-PAEK powder was then directly dissolved in the solution. Finally, DMAC was added into the DMSO solution in a volume fraction of 5% at 30 °C and stirred for 24 hours. The clarified and transparent dispersion was poured onto an 8 cm × 8 cm horizontal glass plate after filtration and heated in an oven at 70 °C for 36 hours to remove the solvent. Afterwards, the membranes were peeled off and then immersed in 0.5 M H₂SO₄ solution at 60 °C for 24 hours, followed by thorough rinsing with deionized water. All membranes were thoroughly dried in vacuum at 60 °C.

Measurements

The chemical structures of DMNF, DFBP, and the polymers were confirmed by ¹H NMR spectroscopy on a Bruker Avance 510 spectrometer, which was conducted with DMSO-d₆ as the solvent and tetramethylsilane (TMS) as the internal standard.

Electron microscope observations

The microstructure and morphology of the membranes were studied by high-resolution transmission electron microscopy (HRTEM) recorded on a JEM-2100F. Before observation, membranes were immersed in 1 M (CH₃COO)₂Pb aqueous solution for 72 hours, then rinsed with deionized water and ultimately dried at room temperature. The stained samples were then embedded in epoxy resin and sectioned with a microtome. Thick samples were placed on copper grids.

Thermal stability

Thermogravimetric analysis (TGA) was performed on a Pyris-1-TGA (PerkinElmer). Before the test, the samples were kept at 120 °C in vacuum for 24 hours to remove moisture. And in the

test, samples were heated from 100 to 800 °C at a speed of 10 °C min⁻¹ in a nitrogen atmosphere in a Pt crucible. The relevant data are shown in Fig. S2.†

Mechanical strength

Tensile strength, Young's modulus, and elongation at break of the membranes were measured at room temperature on a tensile tester (SHIMADZU AG-I 1KN) at a speed of 2 mm min⁻¹.

Liquid adsorption properties

The weight and size (in the area and thickness) of the dry membranes were measured before the test. Then the membranes were soaked in a series of solutions (deionized water, 1 M methanol, 2 M methanol) at 25, 40, 60 and 80 °C for 24 hours, respectively. The liquid uptake (LU) and swelling ratio (SR) of membranes were then obtained using the equations given below:

$$\text{LU} = \frac{W_{\text{wet}} - W_{\text{dry}}}{W_{\text{dry}}} \times 100\% \quad (1)$$

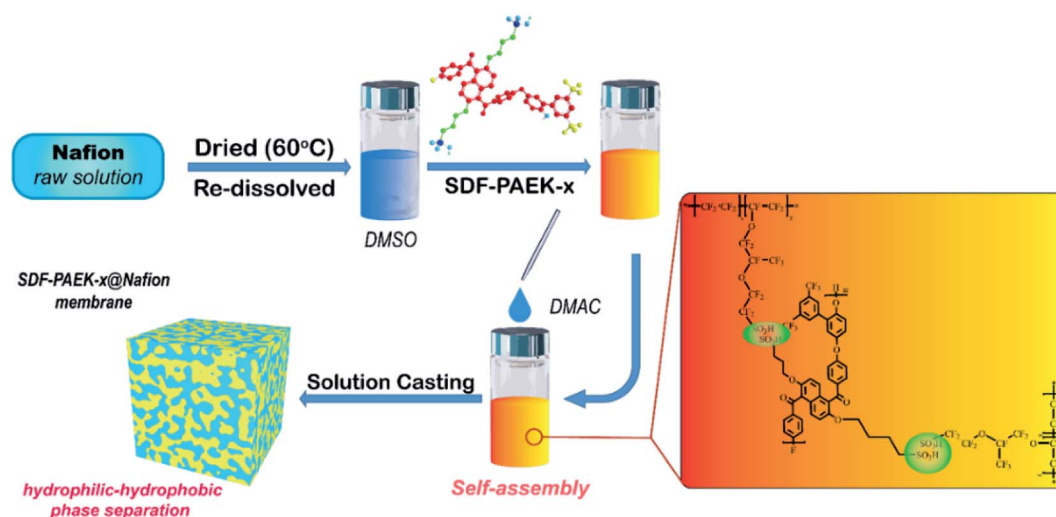
$$\text{SR}_{\text{area}} = \frac{S_{\text{wet}} - S_{\text{dry}}}{S_{\text{dry}}} \times 100\% \quad (2)$$

$$\text{SR}_{\text{thickness}} = \frac{T_{\text{wet}} - T_{\text{dry}}}{T_{\text{dry}}} \times 100\% \quad (3)$$

where W_{wet} and W_{dry} are the weights of wet and dry membranes, S_{wet} and T_{wet} are the area and thickness of wet membranes, respectively. S_{dry} and T_{dry} are the area and thickness of dry membranes, respectively.

Ion exchange capacity (IEC)

The IEC of membranes was determined by titration *via* the method reported previously.³⁶ Firstly, dry membranes were equilibrated in 1 M sodium chloride solution for 72 h to release the protons completely. Afterwards, the solution was titrated



Scheme 1 The preparation procedure of SDF-PAEK@Nafion-x composite membranes.

with standard NaOH solution calibrated with potassium hydrogen phthalate. The IEC titration was carried out three times, and the average value was calculated using:

$$\text{IEC} = \frac{V_{\text{NaOH}} \times C_{\text{NaOH}}}{W_{\text{dry}}} \times 100\% \quad (4)$$

where V_{NaOH} and C_{NaOH} mean the volume (mL) and concentration (mol L^{-1}) of NaOH solution, respectively.

Degree of sulfonation (DS)

DS was calculated using

$$\text{DS} = 2(A_{\text{Hm}}/A_{\text{Ha}}) \quad (5)$$

where A_{Hm} is the integral area of ^1H NMR spectra assigned to the $-\text{OCH}_2-$ groups connected with naphthalene rings, and A_{Ha} is the integral area assigned to the phenyl protons adjacent to carbonyl groups.

Proton conductivity

The proton conductivity (σ) was measured on a Princeton Applied Research Model 2273 potentiostat/galvanostat/FRA via a four-electrode AC impedance method from 100 kHz to 1 Hz. The equation is:

$$\sigma = L/(RWT) \quad (6)$$

where L means the distance between electrodes; R means the membrane resistance; W and T mean the width and thickness of the samples, respectively.

Methanol crossover measurements

The methanol crossover was measured on a Princeton Applied Research Model 2273 potentiostat/galvanostat/FRA via the linear sweep voltammetry (LSV) method combined with a DMFC.³² The value was calculated using:

$$P = \frac{L \times CD_{\text{max}}}{6F \times k \times C_{\text{MeOH}}} \quad (7)$$

where P means the methanol crossover value ($\text{cm}^2 \text{s}^{-1}$), L is the thickness of membranes (cm), CD_{max} means the maximum current of the LSV (mA cm^{-2}), F means Faraday constant (C mol^{-1}), k is the drag correction factor -0.739 (2 M methanol); C_{MeOH} is the concentration of methanol solution-2 M.

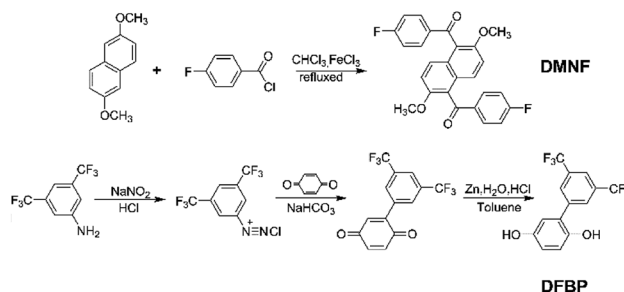
Single-cell performance evaluation

After mixing the catalyst and the Nafion solution at room temperature, it was evenly sprayed on the two sides of the membranes. After drying, the catalyst coated membranes (CCMs) were obtained. Then the gas diffusion layers (GDLs) were sandwiched on both sides of the CCMs. At 80°C , the anode side was supplied with different concentrations of methanol solution (1 M or 2 M) at a rate of 2 mL min^{-1} , and prehumidified oxygen was fed at a rate of 30 mL min^{-1} on the cathode side. The membrane electrode assembly (MEA) was activated at 60°C for 2 hours before the formal test.

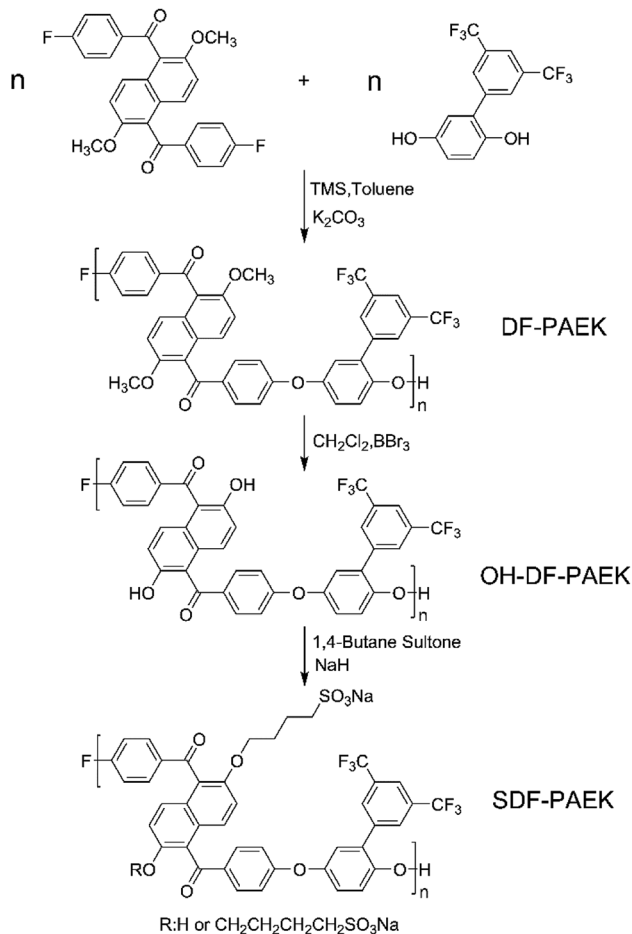
Results and discussion

The synthesis of NFBP, DF-PAEK, and SDF-PAEK-x

As shown in Scheme 2, DMNF was synthesized by the Friedel-Crafts acylation of 2,6-dimethoxynaphthalene with 4-fluorobenzoyl chloride and catalysed by anhydrous ferric chloride according to the method previously reported.³⁷ Through a three-step synthetic process, the synthesis of DFBP was accomplished accordingly. As shown in Scheme 3, SDF-PAEK was synthesized by an aromatic nucleophilic-substitution-polycondensation consisting of three steps. ^1H NMR analysis was used to examine the



Scheme 2 The synthesis procedure of DMNF, DFBP.



Scheme 3 The synthesis procedure of SDF-PAEK.

product in each step, and the results (Fig. 1 and S1†) clearly illustrated changes in molecular structures during the synthetic process. The process from DF-PAEK to OH-DF-PAEK was a demethylation reaction, the conversion of methoxyl groups to hydroxyl groups. Comparing Fig. 1(b) with Fig. 1(c), the chemical shifts of the polymers in the two spectra were consistent. However, there still existed a significant difference, as the characteristic peak of the methoxyl groups attached to the naphthyl groups at 3.76 ppm in Fig. 1(b) completely disappeared in Fig. 1(c); at the same time, the characteristic peak belonging to the phenolic hydroxyl groups was missing in Fig. 1(b) but appeared in Fig. 1(c) (9.86 ppm). This indicates that the methoxyl groups in DF-PAEK had been entirely converted to phenolic hydroxyl groups by a demethylation reaction. Finally, OH-DF-PAEK underwent a grafting reaction in which most of the hydroxyl groups were transformed into flexible pendant side chains with sodium sulfonate. This could be observed by contrasting the ^1H NMR spectrum of SDF-PAEK-1.92

in Fig. 1(c) and (d). In Fig. 1(d), the characteristic peak of the phenolic hydroxyl groups substantially decreased, while the characteristic peaks assigned to methylene groups on the flexible aliphatic chain emerged (4.02, 2.36, 1.55, and 1.46 ppm). The other ^1H NMR peaks remained unchanged. This indicated that SDF-PAEK- x was successfully prepared. Meanwhile, 1.92 as the corresponding value of x , namely DS, could be calculated according to eqn (5).^{34,35}

Morphology study

Fig. 2 shows the typical nanoscale morphology of the membranes. In these TEM images, the black domains represent ion clusters formed by an aggregation of the hydrophilic sulfonic acid groups after Pb^{2+} ion staining. The ion clusters in composite membranes are generally uniform in size and evenly distributed, whereas the ion clusters in recast Nafion are in a high degree of self-aggregation, unequal-sized, and mutually separated. The long flexible aliphatic side chains of SDF-PAEK, containing hydrophilic groups far away from the main chains, show matched size, flexibility, hydrophilicity and chemical affinities to the Nafion side chains. Therefore, in the cast solution, this allows the hydrophilic side chains of different molecules to selectively interact, driving them to aggregate by subordinate-assembly and form nanohydrophilic phase domains with the self-assembly. Similarly, hydrophobic groups of different molecules form hydrophobic domains that are separated from the hydrophilic phase. These TEM images indicate that the microstructures are efficiently regulated in the composite membranes.

The size and distribution of different ion clusters are related to the composition amount of the SDF-PAEK skeleton molecules. It can be observed from Fig. 2(a) and (b) that as the composition amount of the skeleton molecule increases, the dispersed ion

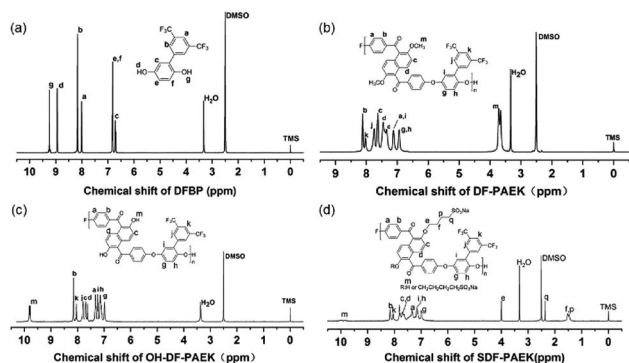


Fig. 1 ^1H NMR spectra of (a) DFBP, (b) DF-PAEK, (c) HO-DF-PAEK, and (d) SDF-PAEK.

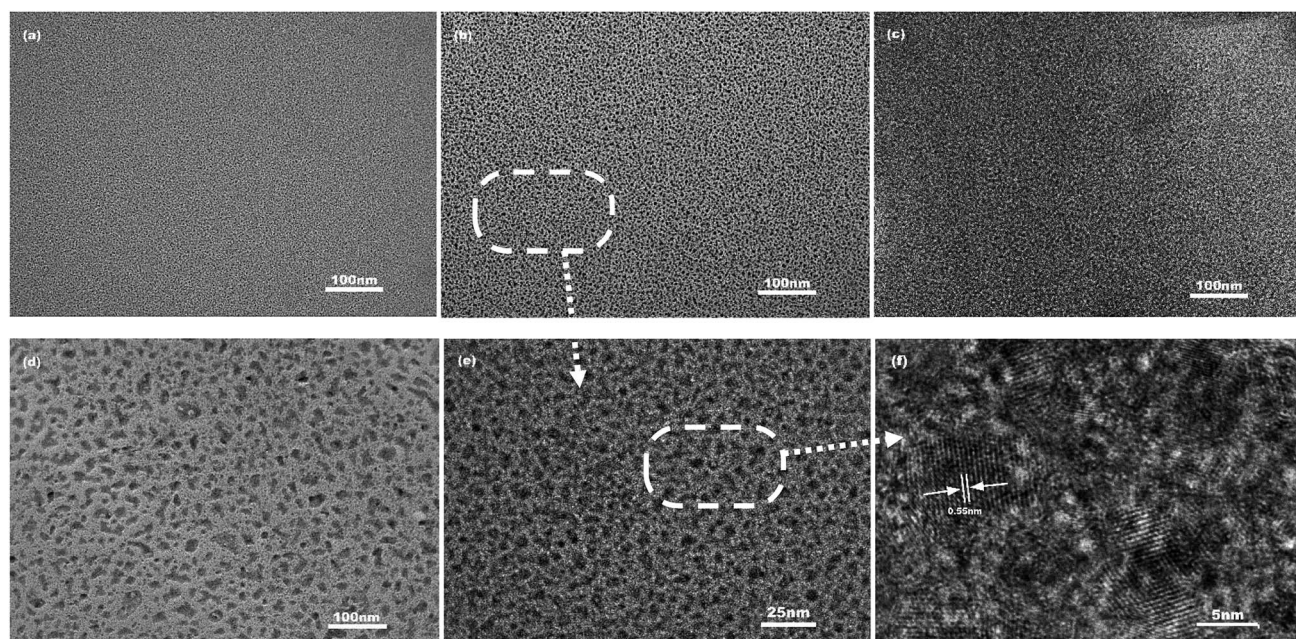


Fig. 2 TEM images of SDF-PAEK@Nafion composite membranes: (a) SDF-PAEK@Nafion-10%; (b, e and f) SDF-PAEK@Nafion-15%; (c) SDF-PAEK@Nafion-20%; (d) recast Nafion.

cluster domains tend to connect, and the scattered ion channels effectively connect. This structure is similar to that of Nafion, but the number of connected channels is larger than that of Nafion. However, in Fig. 2(c), the separation degree of the separated ion clusters significantly increases, and the number of interpenetrating channels decreases. The above results indicate that to some extent, intermolecular thermodynamic incompatibility occurs due to different molecular structures; this intermolecular thermodynamic incompatibility affects the degree of connection among the ion clusters, and therefore, the Nafion must form either a dispersed or a co-continuous morphology to maintain the functionality of the membrane.³⁸ The high magnification observations of SDF-PAEK@Nafion membranes are presented in Fig. 2(e) (250 000x) and Fig. 2(f) (1 500 000x). The apparently ordered lattice structures, in black domains, which possess straight sides and regular ends, are well dispersed and have a narrow distribution in the average size of 5 to 6 nm.³⁹ These results further illustrate that the unique skeleton molecule of SDF-PAEK can facilitate phase separation between hydrophilic and hydrophobic aggregations to form nanochannels, simultaneously promoting proton transport.⁴⁰

Proton conductivity (σ)

The proton conductivity (σ) values measured at different temperatures are displayed in Fig. 3 and Table 1. Proton

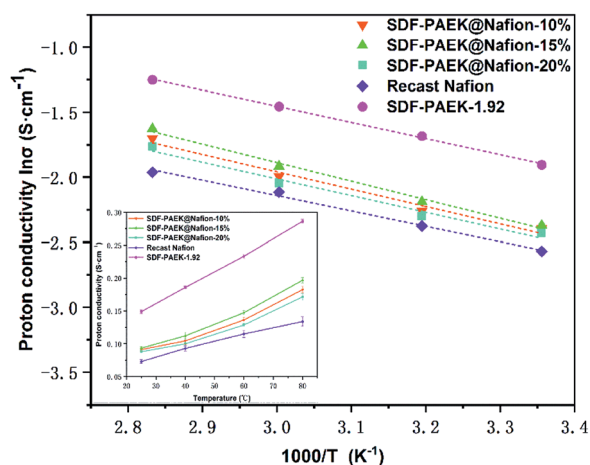


Fig. 3 Proton conductivity of the proton exchange membranes at different temperatures.

conductivity is a vital indicator of PEM properties, which reflects an essential relationship with single-cell performance. As shown in Fig. 3, SDF-PAEK-1.92 showed the highest values of conductivity, and the proton conductivity of composite membranes was much higher than that of recast Nafion. In the SDF-PAEK membrane, a large number of hydrophilic sulfonic acid molecules at the end of side chains could gather together to form the proton channels.⁴¹ When the amount of SDF-PAEK in the composite membranes increased from 10 wt% to 20 wt%, the proton conductivity of SDF-PAEK@Nafion membranes initially experienced an upward trend but then dropped afterward. The addition of skeleton molecules caused the sulfonic acid groups to aggregate; the rigid phenyl and naphthyl rings with the high fluorine content density parts containing the structure in repetitive units came together to form the overall hydrophobic phase domain. As displayed in the TEM images, the proton transport channels induced by the hydrophilic-hydrophobic phase separation were eventually distributed, which significantly promoted proton transport and significantly enhanced proton conductivity.

Nevertheless, intermolecular incompatibility existed between the SDF-PAEK containing rigid groups and the flexible chain-based Nafion molecules. The incompatibility increased as the composition amount of SDF-PAEK increased, thus separating some of the small scattered ion clusters from each other. An extension of the distance between two adjacent proton transport groups would shorten the hydrogen bond lifetime in the transport channels of the fluorination system.⁴² Accordingly, when the temperature increased, membranes with a closer distance between the internal sulfonic acid groups would possess a higher conductivity. The measured experimental data confirmed the above statements—with 15 wt% skeleton molecules, the material exhibited the highest proton conductivity of 0.197 S cm^{-1} at 80°C .

Liquid uptake (LU) and swelling ratio (SR) of membranes

To study the effects of different methanol concentrations on LU and SR, the membranes were immersed in 0 M (deionized water), 1 M and 2 M methanol aqueous solutions at different temperatures. As shown in Fig. 4, Tables S1–S3,[†] the trends of LU and SR are similar. The LU and SR increased with increase in temperature and methanol concentration, respectively. After immersion in DI water, the LU and SR values of recast Nafion membrane appeared to be lower than those of composite

Table 1 The thickness (μm), IEC, proton conductivity (σ), maximum current density (CD_{max}), methanol permeability (P) and selectivity (ϕ) of membranes

Samples	Thickness (μm)	IEC (mequiv g^{-1})	σ (S cm^{-1})		CD_{max} (mA cm^{-2})	P ($10^{-6} \text{ cm}^2 \text{ s}^{-1}$)	ϕ (10^4 S s cm^{-3})
			25°C	80°C			
SDF-PAEK@Nafion-10%	52.67	0.79	0.091 ± 0.003	0.183 ± 0.005	227.90	2.13	8.56
SDF-PAEK@Nafion-15%	49.33	0.86	0.093 ± 0.002	0.197 ± 0.004	203.48	2.03	9.73
SDF-PAEK@Nafion-20%	49.33	0.93	0.087 ± 0.002	0.171 ± 0.005	265.64	2.67	6.42
Recast Nafion	52.33	0.65	0.077 ± 0.001	0.140 ± 0.002	387.46	4.08	3.71

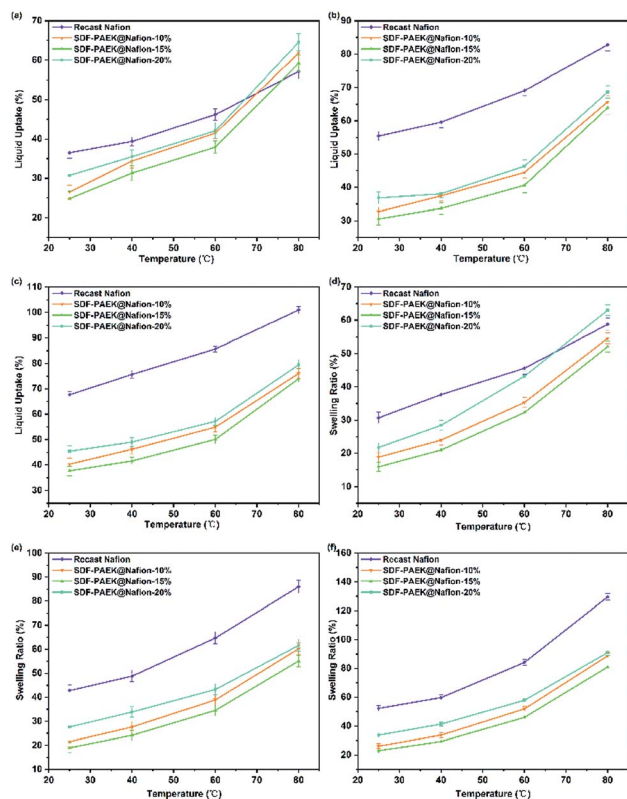


Fig. 4 LU of PEMs at different concentrations: DI water (a), 1 M (b) and 2 M (c) methanol; SR (in area) of PEMs at different concentrations: DI water (d), 1 M (e) and 2 M (f) methanol.

membranes at 80 °C. This may be due to the incompatibility between the Nafion matrix and SDF-PAEK skeleton molecules. A complete interpenetrating network structure could not be formed, and there was certainly void space among the molecules. At higher temperatures, the number of physically cross-linked networks between the different aggregated phases was reduced to a certain degree, so that more water molecules were allowed to enter the membrane interior.

However, in methanol solution, the LU and SR of Nafion were higher than that of composite membranes at each temperature, as Nafion showed a higher affinity to methanol than SDF-PAEK and absorbed more methanol molecules.⁴³ Moreover, skeleton molecules inhibited the degree of matrix swelling; strong intermolecular forces and physical crosslinking between macromolecules limited the mutual penetration among Nafion, H₂O, and methanol molecules. As the additional amount of SDF-PAEK increased from 10% to 15%, all the LU and SR values of composite membranes decreased. When this amount reached 20%, the negative effects of incompatibility were further highlighted: the degrees of molecular separation and the void space among different phase molecules increased. In summary, SDF-PAEK as a skeleton molecule of the membrane can limit the swelling effect of Nafion molecules in methanol aqueous solutions, thus enhancing the dimensional stability of the membrane for DMFCs which work in the environment of methanol aqueous solutions.

Methanol permeability and selectivity

High methanol permeability stands for high methanol cross-over which can degrade the fuel efficiency and single-cell performance of DMFCs. Therefore, reducing fuel permeability is a vital method to improve DMFC performance.^{21,44} The results of the LSV of the methanol resistance of MEAs are shown in Fig. 5 and Table 1. The 2 M methanol solution was introduced into the anode side, and at 80 °C, recast Nafion exhibited the largest CD_{max} of 387.46 mA cm⁻². The above result indicated that under these conditions, the methanol resistance efficiency of the composite membranes was higher than that of Nafion. As the SDF-PAEK composition increased from 10% to 15%, the CD_{max} of the composite membrane decreased from 227.90 mA cm⁻² to 203.48 mA cm⁻², which indicated that skeleton molecules exhibited some enhancement effects on the methanol resistance of composite membranes.⁴⁵ However, with the addition of skeleton molecules further increased from 15% to 20%, CD_{max} increased to 265.64 mA cm⁻², due to the separation of molecules inducing a larger void space inside the membrane and thus increasing the methanol permeability.

It is also essential to maintain sufficient proton conductivity while reducing methanol permeability. Combined with the proton conductivity, the selectivity of the materials was calculated. The selectivity value of SDF-PAEK@Nafion-15% (9.73×10^4 S s cm⁻³) was more than 1.5 times higher than that of recast Nafion (3.71×10^4 S s cm⁻³). The penetration of methanol is also inseparable from proton transport channels. As shown in Fig. 5(c), the distinctive aggregation–separation of hydrophilic–hydrophobic phases and the characteristic functional groups of the composite membranes play a vital role in the selection of

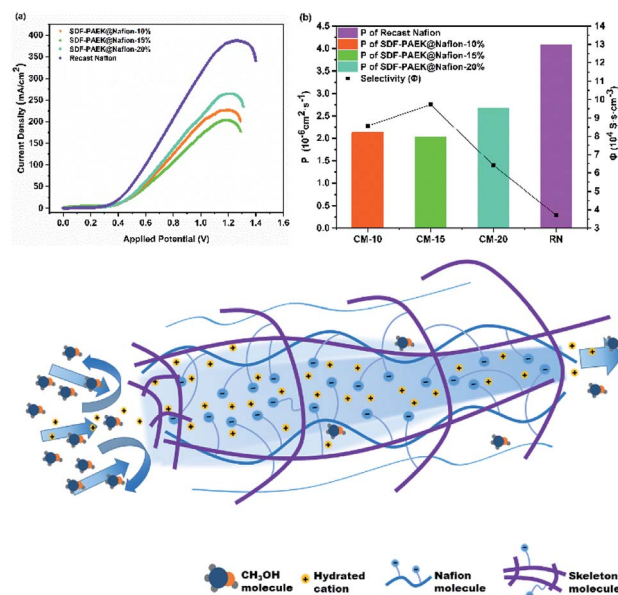


Fig. 5 (a) The LSV curves of membranes for testing methanol cross-over at 80 °C, (b) methanol permeability (P) and selectivity (ϕ) of composite membranes (CM) and recast Nafion (RN); (c) schematic diagram for the proton transport channel of the prepared membranes.

Table 2 The mechanical properties of PEMs, OCV values and PD_{\max} of DMFCs at different methanol concentrations (80 °C)

Samples	OCV (V)		PD_{\max} (mW cm ⁻²)		Tensile strength (MPa)	Young's modulus (MPa)	Elongation at break (%)
	1 M	2 M	1 M	2 M			
SDF-PAEK@Nafion-10%	0.763	0.678	107	128	16.5 ± 1.6	237 ± 26	170 ± 11
SDF-PAEK@Nafion-15%	0.812	0.730	112	139	14.4 ± 0.6	291 ± 15	160 ± 16
SDF-PAEK@Nafion-20%	0.726	0.617	96	113	15.2 ± 0.7	312 ± 13	125 ± 23
Recast Nafion	0.676	0.528	81	94	13.7 ± 0.3	240 ± 20	154 ± 5

methanol and protons. In this way, the selectivity of the composite membrane can be higher than that of recast Nafion.

Mechanical properties

As shown in Table 2, the comprehensive mechanical performances of composite membranes are better than those of recast Nafion. Tensile strength is the critical value of the transition from uniform plastic deformation to locally concentrated plastic deformation when membranes are stretched. In contrast to recast Nafion, SDF-PAEK containing rigid phenyl and naphthyl rings served as the reinforcement site; therefore, composite membranes incorporating skeleton molecules could reach higher tensile strength.^{44,46} However, there was some incompatibility between SDF-PAEK and Nafion molecules. When the addition amount of SDF-PAEK was relatively high, for example, up to 20%, the negative effects of intermolecular incompatibility resulted in a reduction in material density and mechanical strength.⁴⁷

Electrochemical behaviour

According to the DMFC equivalent circuit (Fig. 6(c)), different single cells were investigated to obtain the Nyquist plots at 0.25 V and 80 °C. The components of the equivalent circuit are as follows: R_{Ω} is the high-frequency resistance, L is the pseudo inductance, R_{ct} is the charge transfer resistance, R_{mt} is the mass

transport resistance, and CPE_1 and CPE_2 are the constant phase elements connected in parallel with charge transfer and mass transport resistances. From Fig. 6(a), (b) and S5,[†] it can be observed that as the concentration of methanol solutions increased, the radius of each impedance arc decreased, which reveals the improvement in the methanol oxidation reaction and the restriction on the oxygen reduction reaction, since a small amount of methanol that crossed over from the anode side sharply restricted the transport of protons to the cathode side.⁴⁸ The ohmic resistance values of the different materials were close, whereas the polarization resistance values of the fuel cell fabricated with recast Nafion were the highest of those determined here. The addition of skeleton molecules caused the impedance arcs of membranes to converge. However, for composite membranes, as the amount of SDF-PAEK increased, the polarization resistance presented a similar growing trend as well, which might be related to the incompatibility between the rigid molecules of SDF-PAEK and the flexible aliphatic chain molecules of Nafion. It is worth noting that the charge-transfer resistances of the three composite membranes increased after an initial drop as the amount of SDF-PAEK increased from 10% to 15%. The composite membrane with a 15% composition amount requires the lowest resistance to charge transfer, which was consistent with its highest proton conductivity.^{36,49} In the high-frequency region, small arcs with the centers below the real axis appear in the Nyquist plots, suggesting that a dispersion effect may occur at the same time. The capacitance frequency response characteristics of the solid electrode double layers display inconsistency and deviation with the pure capacitance to some extent. There was a certain degree of nonuniformity between composite membranes with catalyst layers, and it was lower than that between the Nafion membrane and catalyst layers.

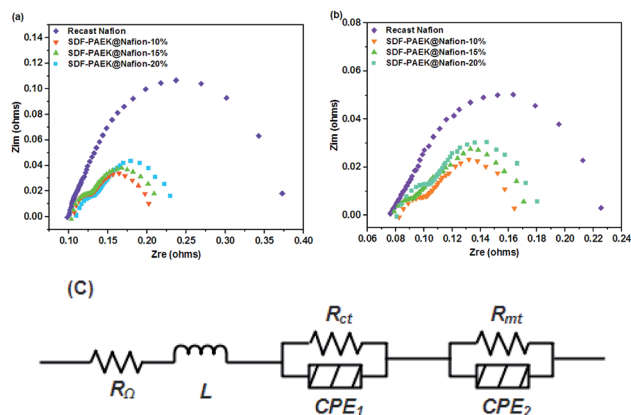


Fig. 6 Nyquist plots of single cell impedance spectra for (a) 1 M methanol solution, (b) 2 M methanol solution, and (c) the DMFC equivalent circuit for the evaluation of the measured impedance spectra.

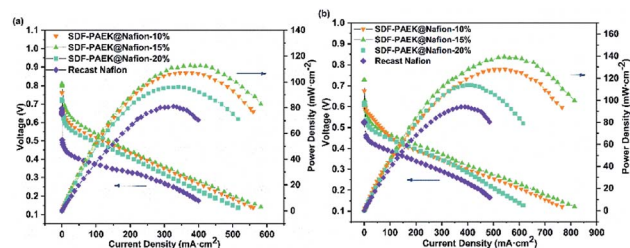


Fig. 7 The polarization and power density curves with different methanol solution concentrations at 80 °C: (a) $C_{MeOH} = 1$ M, and (b) $C_{MeOH} = 2$ M.

Table 3 DMFC performances for different kinds of composite membranes

Samples	T^a (°C)	C_{MeOH} (M)	OCV (V)	PD_{max} (mW cm ⁻²)
SDF-PAEK@Nafion-15% [this work]	80	2	0.730	139
Nafion-sulfonated silica ⁵⁹	60	1	0.84	130
Nafion-zeolite hybrid ⁶⁰	70	1	0.71	98
Nafion-mordenite hybrid ⁶¹	70	1	0.6	80
SPEEK/sSrZrO ₃ (3 wt%) ¹²	80	2	0.82	110
SPVDF-co-HFP/SPA ⁶²	60	2	0.79	20.7
<i>p</i> -BPAF@Nafion-7.5 (ref. 24)	80	2	0.836	111.53
N/PVFP-BI-9.5-0.5 (ref. 63)	80	2	0.541	103.0
NP-composite ²³	70	2	0.52	84.5
Nafion-TiO ₂ hybrid ¹³	80	2	0.58	28
Nafion-GO platelet hybrid ⁶⁴	90	2	0.7	120
Nafion/SNPAEK-7.5% (ref. 65)	80	2	0.77	47
C-PEEK-25 (ref. 66)	25	4	0.8	35.3

^a The operating temperature of DMFC mentioned in references.

The radius values of the arcs correspond to the ionic impedance of PEMs. An increase in the impedance of any other parts of the cell causes the semi-circular arc to move toward the low-frequency region.^{36,50-52} The electrochemical impedance test of DMFC shows a series of uncertainties, and related research needs further exploration. In summary, the composite membrane after incorporating skeleton molecules in the Nafion membrane possessed lower proton transfer impedance than recast Nafion.

Different concentrations of methanol solution were fed into the anode sides at 25 °C and 80 °C to conduct DMFC polarization studies on different membranes. The corresponding OCV and power density data are shown in Fig. 7, S6† and Table 2. It is easy to find that with the increase of methanol concentration, the OCV values of all MEAs were reduced, because of more fuel permeating through the membrane from the anode sides to the cathode sides. And the fuel permeation led to an increase in methanol crossover and inverse voltage, thus resulting in higher depolarization losses of the OCV. However, under the same conditions, composite membranes exhibited better methanol resistance and reduced depolarization losses in comparison with the values of recast Nafion membranes, so the OCV values of composite membranes were higher than that of recast Nafion.⁵³⁻⁵⁵ The SDF-PAEK@Nafion-15% membrane showed the highest OCV (0.812 V, 2 M), which was consistent with the highest conductivity test results.

However, when the methanol concentration increased from 1 M to 2 M, the maximum power density (PD_{max}) values of all membranes were improved. This indicated that the positive impact of increasing fuel concentration was greater than the negative impact of increased methanol crossover. Under the condition of 2 M methanol solution, the PD_{max} of the SDF-PAEK@Nafion-15% membrane reached 139 mW cm⁻² at 80 °C. In the composite membrane, Nafion molecules were restructured around skeleton molecules, where the ion clusters tended toward aggregation. More proton transport channels interconnected (verified by HRTEM images) and thus exhibited higher affinity toward hydration molecules.^{56,57} At the same time, due to the dense hydrophobic domains, the methanol

crossover can be reduced, which decreased the depolarization losses and then improved the power density.⁵⁸ The low fuel cell performance revealed the proton-transport problem in the high current density region at a concentration of 1 M, whereas at a concentration of 2 M, the reduced concentration polarization improved cell performance at high current density. Under the same conditions, the PD_{max} of the 15% composite membranes was higher than that of the 10% composite membranes. However, for the 20% composite membrane, the negative effect of the incompatibility between the rigid backbone structure of SDF-PAEK molecules and the flexible backbone of Nafion molecules was highlighted, resulting in a decrease in power density. This was consistent with the test results of EIS.

Furthermore, comparison of DMFC performance between SDF-PAEK@Nafion-15% and other polymer membranes reported in previous literature was made, and the results are summarized in Table 3. It can be seen that the composite membrane SDF-PAEK@Nafion-15% exhibits a comparable and even better single-cell performance.

Conclusions

A series of SDF-PAEK@Nafion-*x* membranes, as novel PEM materials suitable for DMFC application, were prepared by incorporating a novel SDF-PAEK skeleton molecule into Nafion membranes. Compared to recast Nafion, the cost of composite membranes was reduced dramatically since the composition can reach 20%. Moreover, skeleton molecules promoted the automatic aggregation-separation of hydrophilic-hydrophobic phases by self-assembly, thus enhancing the proton conductivity of composite membranes. The TEM analyses demonstrated the existence and even distribution of ion cluster microphase lattices and bicontinuous proton transport channels. At 80 °C, the proton conductivity of SDF-PAEK@Nafion-15% was 0.197 S cm⁻¹, whereas the methanol permeability value was reduced by half over that of the recast Nafion. The composite membrane thus exhibited a 2.6-fold increase in selectivity. The addition of SDF-PAEK also enhanced the mechanical strength and dimensional stability of composite

membranes. The SR value of the composite membrane was 38% of that of the recast Nafion (in area, 2 M aqueous methanol solution), significantly reducing the manufacturing difficulties of the MEA. The single-cell performance test showed that the PD_{\max} of PAEK@Nafion-15% was 139 mW cm^{-2} (at $80 \text{ }^\circ\text{C}$, 2 M methanol aqueous solution), which was much higher than that of the recast Nafion with a maximum power density of 94 mW cm^{-2} . All these results demonstrate that composite membranes have the potential to be used as PEMs for DMFC applications, and this provides opportunities to research and develop alternative PEMs by incorporating skeleton molecules into the Nafion matrix.

Conflicts of interest

There are no conflicts to declare.

Acknowledgements

We acknowledge the financial support from the Natural Science Foundation of China (No. 21875088).

References

- N. Li, C. Wang, S. Y. Lee, C. H. Park, Y. M. Lee and M. D. Guiver, *Angew. Chem., Int. Ed.*, 2011, **50**, 9158–9161.
- D. Guo, A. N. Lai, C. X. Lin, Q. G. Zhang, A. M. Zhu and Q. L. Liu, *ACS Appl. Mater. Interfaces*, 2016, **8**, 25279–25288.
- C. Wang, N. Li, D. W. Shin, S. Y. Lee, N. R. Kang, Y. M. Lee and M. D. Guiver, *Macromolecules*, 2011, **44**, 7296–7306.
- N. R. Kang, S. Y. Lee, D. W. Shin, D. S. Hwang, K. H. Lee, D. H. Cho, J. H. Kim and Y. M. Lee, *J. Power Sources*, 2016, **307**, 834–843.
- L. Lei, X. Zhu, J. Xu, H. Qian, Z. Zou and H. Yang, *J. Power Sources*, 2017, **350**, 41–48.
- X. Wang, S. Wang, C. Liu, J. Li, F. Liu, X. Tian, H. Chen, T. Mao, J. Xu and Z. Wang, *Electrochim. Acta*, 2018, **283**, 691–698.
- J. Zheng, Q. He, C. Liu, T. Yuan, S. Zhang and H. Yang, *J. Membr. Sci.*, 2015, **476**, 571–579.
- A. L. Mong, S. Yang and D. Kim, *J. Membr. Sci.*, 2017, **543**, 133–142.
- M. Sadakiyo, H. Okawa, A. Shigematsu, M. Ohba, T. Yamada and H. Kitagawa, *J. Am. Chem. Soc.*, 2012, **134**, 5472–5475.
- M. Liu, L. Chen, S. Lewis, S. Y. Chong, M. A. Little, T. Hasell, I. M. Aldous, C. M. Brown, M. W. Smith, C. A. Morrison, L. J. Hardwick and A. I. Cooper, *Nat. Commun.*, 2016, **7**, 12750.
- H. Xu, S. Tao and D. Jiang, *Nat. Mater.*, 2016, **15**, 722–726.
- G. Gnana kumar and A. Manthiram, *J. Mater. Chem. A*, 2017, **5**, 20497–20504; C. de Bonis, D. Cozzi, B. Mecheri, A. D'Epifanio, A. Rainer, D. De Porcellinis and S. Licocchia, *Electrochim. Acta*, 2014, **147**, 418–425.
- C. de Bonis, D. Cozzi, B. Mecheri, A. D'Epifanio, A. Rainer, D. De Porcellinis and S. Licocchia, *Electrochim. Acta*, 2014, **147**, 418–425.
- W. Zhengbang, H. Tang and P. Mu, *J. Membr. Sci.*, 2011, **369**, 250–257.
- F. Meng, N. V. Aieta, S. F. Dec, J. L. Horan, D. Williamson, M. H. Frey, P. Pham, J. A. Turner, M. A. Yandrasits, S. J. Hamrock and A. M. Herring, *Electrochim. Acta*, 2007, **53**, 1372–1378.
- J. L. Malers, M.-A. Sweikart, J. L. Horan, J. A. Turner and A. M. Herring, *J. Power Sources*, 2007, **172**, 83–88.
- J. R. Ferrell III, M.-C. Kuo, J. A. Turner and A. M. Herring, *Electrochim. Acta*, 2008, **53**, 4927–4933.
- H. Beydaghi, M. Javanbakht, B. Ahmad, ab P. Salarizadeh, H. Ghafarian-Zahmatkesh, S. Kashefi and E. Kowsari, *RSC Adv.*, 2015, **5**, 74054–74064.
- D. He, H. Tang, Z. Kou, M. Pan, X. Sun, J. Zhang and S. Mu, *Adv. Mater.*, 2017, **29**, 1601741.
- G. Rambabu, N. Nagaraju and S. D. Bhat, *Chem. Eng. J.*, 2016, **306**, 43–52.
- Y. Zhang, W. Cai, F. Si, J. Ge, L. Liang, C. Liu and W. Xing, *Chem. Commun.*, 2012, **48**, 2870.
- A. K. Sahu, S. Meenakshi, S. D. Bhat, A. Shahid, P. Sridhar, S. Pitchumani and A. K. Shukla, *J. Electrochem. Soc.*, 2012, **159**, F702–F710.
- H. Lin, T. L. Yu, L. Huang, L. Chen, K. Shen and G. Jung, *J. Power Sources*, 2005, **150**, 11–19.
- C. Ru, Y. Gu, Y. Duan, C. Zhao and H. Na, *J. Membr. Sci.*, 2019, **573**, 439–447.
- A. Guimet, L. Chikh, A. Morin and O. Fichet, *J. Membr. Sci.*, 2016, **514**, 358–365.
- P. Prapainainar, Z. Du, P. Kongkachuichay, S. M. Holmes and C. Prapainainar, *Appl. Surf. Sci.*, 2017, **421**, 24–41.
- T. Y. Inan, H. Doğan, E. E. Unveren and E. Eker, *Int. J. Hydrogen Energy*, 2010, **35**, 12038–12053.
- C. H. Park, S. Y. Lee, D. S. Hwang, D. W. Shin, D. H. Cho, K. H. Lee, T. Kim, T. Kim, M. Lee, D. Kim, C. M. Doherty, A. W. Thornton, A. J. Hill, M. D. Guiver and Y. M. Lee, *Nature*, 2016, **532**, 480–483.
- K. A. Mauritz and R. B. Moore, *Chem. Rev.*, 2004, **104**(10), 4535–4586.
- K. S. Siegert, F. R. Lange, E. R. Sittner, H. Volker, C. Schlockermann, T. Siegrist and M. Wuttig, *Rep. Prog. Phys.*, 2015, **78**, 13001.
- K. Kreuer and G. Portale, *Adv. Funct. Mater.*, 2013, **23**, 5390–5397.
- S. Kundu, M. W. Fowler, L. C. Simon and S. Grot, *J. Power Sources*, 2006, **157**, 650–656.
- Z. Xu, Z. Qi and A. Kaufman, *J. Power Sources*, 2003, **115**, 49–53.
- B. Wang, L. Hong, Y. Li, L. Zhao, C. Zhao and H. Na, *ACS Appl. Mater. Interfaces*, 2017, **9**, 32227–32236.
- C. Ru, Y. Gu, Y. Duan, C. Zhao and H. Na, *J. Membr. Sci.*, 2019, **573**, 439–447.
- J. P. Diard, B. Le Gorrec, C. Montella, C. Poinignon and G. Vitter, *J. Power Sources*, 1998, **74**, 244–245.
- K. Shao, J. Zhu, C. Zhao, X. Li, Z. Cui, Y. Zhang, H. Li, D. Xu, G. Zhang, T. Fu, J. Wu and W. Xing, *J. Polym. Sci., Part A: Polym. Chem.*, 2009, **47**, 5772–5783.

- 38 G. He, Z. Li, J. Zhao, S. Wang, H. Wu, M. D. Guiver and Z. Jiang, *Adv. Mater.*, 2015, **27**, 5280–5295.
- 39 D. A. Tomalia, A. M. Naylor and A. William, *Angew. Chem., Int. Ed. Engl.*, 1990, **29**, 138–175.
- 40 C. Wang, D. W. Shin, S. Y. Lee, N. R. Kang, G. P. Robertson, Y. M. Lee and M. D. Guiver, *J. Mater. Chem.*, 2012, **22**, 25093.
- 41 T. D. Gierke, G. E. Munn and F. C. J. Wilson, *J. Polym. Sci., Polym. Phys. Ed.*, 1981, **19**, 1687–1704.
- 42 Y. Song, J. Huo, N. Zhang, J. Bao, X. Zhang, X. Ruan and G. He, *J. Phys. Chem. C*, 2018, **122**, 1982–1989.
- 43 M. Gil, X. Ji, X. Li, H. Na, J. Eric Hampsey and Y. Lu, *J. Membr. Sci.*, 2004, **234**, 75–81.
- 44 M. Han, G. Zhang, K. Shao, H. Li, Y. Zhang, M. Li, S. Wang and H. Na, *J. Mater. Chem.*, 2010, **20**, 3246.
- 45 X. Ren, T. E. Springer, T. A. Zawodzinski and S. Gottesfeld, *J. Electrochem. Soc.*, 2000, **147**(2), 466–474.
- 46 H. Lin, C. Zhao, Y. Jiang, W. Ma and H. Na, *J. Power Sources*, 2011, **196**, 1744–1749.
- 47 S. Shi, G. Chen, Z. Wang and X. Chen, *J. Power Sources*, 2013, **238**, 318–323.
- 48 S. M. Rezaei Niya and M. Hoorfar, *J. Power Sources*, 2013, **240**, 281–293.
- 49 S. M. Rezaei Niya, R. K. Phillips and M. Hoorfar, *J. Electroanal. Chem.*, 2016, **775**, 273–279.
- 50 J. T. Mueller and P. M. Urban, *J. Power Sources*, 1998, **75**, 139–143.
- 51 S. Yang, C. Chen and W. Wang, *J. Power Sources*, 2010, **195**, 2319–2330.
- 52 S. Asghari, A. Mokmeli and M. Samavati, *Int. J. Hydrogen Energy*, 2010, **35**, 9283–9290.
- 53 F. A. Zakil, S. K. Kamarudin and S. Basri, *Renewable Sustainable Energy Rev.*, 2016, **65**, 841–852.
- 54 B. Bae, T. Yoda, K. Miyatake, H. Uchida and M. Watanabe, *Angew. Chem., Int. Ed.*, 2010, **49**, 317–320.
- 55 G. Gnana Kumar, *J. Mater. Chem.*, 2011, **21**, 17382.
- 56 M. Ranjani, D. J. Yoo and G. Gnana Kumar, *J. Membr. Sci.*, 2018, **555**, 497–506.
- 57 G. Gnana kumar and A. Manthiram, *J. Mater. Chem. A*, 2017, **5**, 20497–20504.
- 58 G. Gnana Kumar, J. Shin, Y. Nho, I. S. Hwang, G. Fei, A. R. Kim and K. S. Nahm, *J. Membr. Sci.*, 2010, **350**, 92–100.
- 59 J. Kim, S. Kim, K. Nam and D. Kim, *J. Membr. Sci.*, 2012, **415–416**, 696–701.
- 60 Z. Chen, B. Holmberg, W. Li, X. Wang, W. Deng, R. Munoz and Y. Yan, *Chem. Mater.*, 2006, **18**, 5669–5675.
- 61 S. Al-Batty, C. Dawson, S. P. Shanmukham, E. P. L. Roberts and S. M. Holmes, *J. Mater. Chem. A*, 2016, **4**, 10850–10857.
- 62 K. Dutta, S. Das and P. P. Kundu, *J. Membr. Sci.*, 2015, **473**, 94–101.
- 63 S. Wang and H. Lin, *J. Power Sources*, 2014, **257**, 254–263.
- 64 I. Nicotera, C. Simari, L. Coppola, P. Zygouri, D. Gournis, S. Brutti, F. D. Minuto, A. S. Aricò, D. Sebastian and V. Baglio, *J. Phys. Chem. C*, 2014, **118**, 24357–24368.
- 65 B. Wang, L. Hong, Y. Li, L. Zhao, C. Zhao and H. Na, *ACS Appl. Mater. Interfaces*, 2017, **9**, 32227–32236.
- 66 L. Lei, X. Zhu, J. Xu, H. Qian, Z. Zou and H. Yang, *J. Power Sources*, 2017, **350**, 41–48.